Frictional interpretation of thermodynamic transport parameters for porous nanofiltration membranes

Ramesh R. Sharma and Shankararaman Chellam

ABSTRACT

Phenomenological coefficients arising from the application of irreversible thermodynamics to the passage of water and dilute solutions of alcohols, sugars, NaCl and $NaClO_4$ across two commercially available nanofiltration membranes are physically interpreted using the frictional model proposed by Spiegler, Kedem and Katchalsky. The effects of temperature in the range 5–41°C and NaCl concentration in the range 1–50 meq l^{-1} were also quantified. Pure water permeability, solute reflection coefficient and solute diffusive permeability are linked to solute–water, solute–membrane and water–membrane frictional interactions within the nanofilters' polymeric network. Changes in intra-membrane frictional coefficients with feed water temperature and concentration are related to variations in nanofilter morphological and charge characteristics. As may be expected, water–membrane friction coefficients were several orders of magnitude smaller than solute–membrane friction coefficients demonstrating that the semi-permeable nanofilters hindered solute passage to a substantially greater degree than water. Analogous to viscosity, all frictional coefficients decreased with temperature. Greater steric hindrances faced by larger solutes to passage across nanofilters are manifested as increasing activation energies of solute–membrane interactions and solute–water interactions. Hydrodynamic theories of hindered transport are shown to closely follow trends in frictional coefficients with increasing solute size. Antagonistic effects of changes in electrostatic and steric interactions with temperature reduced activation energies of electrolyte–membrane frictional interactions.

Key words | activated transport, irreversible thermodynamics, membrane transport phenomena, nanofiltration, polymeric membranes

Ramesh R. Sharma
Department of Civil and Environmental Engineering,
4800 Calhoun Road, University of Houston,
Houston, TX 77204-4003,
USA
Phone: (713) 743-4265
Fax: (713) 743-4260

Shankararaman Chellam (corresponding author)
Department of Civil and Environmental Engineering, and
Department of Chemical Engineering,
4800 Calhoun Road, University of Houston,
Houston, TX 77204-4003,
USA
Phone: (713) 743-4265
Fax: (713) 743-4260
E-mail: *chellam@uh.edu*

INTRODUCTION

Delineating transport mechanisms of solutes and water across porous nanofiltration (NF) membranes is an active research area partially due to their recent invention and the growing interest in implementing them for environmental separations. Approaches based on irreversible thermodynamics (Kedem & Katchalsky 1958; Spiegler & Kedem 1966) and the (extended) Nernst-Planck Equation (Lakshminarayanaiah 1969; Dresner 1972; Bowen & Mukhtar 1996) are popular to model permselectivity and water permeability of NF membranes. A major shortcoming of the irreversible thermodynamics approach is that it does not provide insights into molecular level interactions. In contrast, mechanistic interpretations of membrane transport phenomena are possible from the extended Nernst-Planck equation because it explicitly incorporates hindered convection, diffusion and electromigration. However, idealizations of membrane pore size (distribution), pore geometry and charge density are necessary to physically interpret phenomenological coefficients arising from non-equilibrium thermodynamics and numerically solve the extended

doi: 10.2166/aqua.2006.037

Nernst-Planck equation. For example, pore size distributions of ultrafiltration (Mochizuki & Zydney 1993; Combe *et al.* 1999) and NF membranes (Van der Bruggen *et al.* 2000; Seidel *et al.* 2001; Nghiem *et al.* 2004; Sharma & Chellam 2005) as well as charge characteristics (Wang *et al.* 1995b; Bowen & Mukhtar 1996) have been obtained assuming straight cylindrical or slit pores and that surface charge is homogeneously distributed.

Physical interpretations of macroscopic phenomenological coefficients without assumptions and idealizations regarding membrane morphology, pore size distributions, pore shapes, charge density, etc. are possible in terms of intra-membrane frictional interactions (Kedem & Katchalsky 1961; Ginzburg & Katchalsky 1963; Kaufmann & Leonard 1968; Kokubo & Sakai 1998). In this 'intermediate' approach, two-way interactions between solute, water and the membrane are captured as solute–water, solute–membrane and water–membrane frictional coefficients, which cumulatively include steric, viscous, polar and electrical interactions. Because quantitative measures of the relative importance of solute–membrane, solute–water and membrane–water interactions in tortuous pores of irregular shape and cross-section with heterogeneous charge density can be obtained, the frictional approach is employed in this research.

Transport phenomena considered in this paper are based on two driving forces (pressure and concentration gradients) that result in three fluxes (water flux, solute diffusion and coupled convection of water and solute). Explicitly incorporating more driving forces (e.g. electric potential gradient) in the irreversible thermodynamics approach will increase the number of independent phenomenological coefficients to nine for single-salt solutions. Onsager's reciprocal theorem reduces the number of unknown coefficients to six due to symmetry (Kedem & Katchalsky 1958, 1961). Next, NF experiments can be designed to directly obtain pure water permeability, reflection coefficient and diffusive permeability (Wang *et al.* 1995a; Van der Bruggen & Vandecasteele 2002; Sharma *et al.* 2003). Hence, three more coefficients (electroosmotic parameter, ion transport number and membrane conductivity) need to be independently measured for rigorous analysis of salt transport (Meares *et al.* 1972). To eliminate the additional experimental burden associated with measurements of these three additional coefficients and because cation and anion fluxes are identical in single (1-1) salt systems to maintain electroneutrality (Szanuawska & Spencer 1997; Yang & Liu 1998; Yamauchi *et al.* 1999), we have combined individual cation and anion friction coefficients into a single salt friction coefficient for 1-1 electrolytes following commonly accepted protocols (e.g. Szanuawska & Spencer 1997; Yang & Liu 1998; Yamauchi *et al.* 1999). Importantly, this facilitates a direct comparison of neutral solute and electrolyte permeation across NF membranes.

Further, only limited mechanistic information on temperature effects on membrane selectivity is available in the existing literature even though NF and reverse osmosis (RO) membranes often operate on surface waters and surficial groundwaters whose temperature varies over time and with season (Chellam *et al.* 1997; Ventresque *et al.* 1997; Taniguchi & Kimura 2000; Abdel-Jawad *et al.* 2001). This paper is amongst our recent investigations of temperature effects on transport phenomena across water treatment NF membranes (Sharma *et al.* 2003; Sharma & Chellam 2005, 2006). Paradoxically, concentration effects on NF frictional coefficients have also not been thoroughly studied to date even though this is also an important environmental parameter.

The principal objective of this research is to quantify the effects of temperature and concentration on frictional coefficients within the polymeric matrix of thin-film composite membranes. Solute reflection coefficients, diffusive solute permeabilities and water permeabilities of two commercially available nanofilters are linked to interactions between solutes (alcohols, sugars, NaCl and $NaClO_4$), membranes and water. Variations of frictional coefficients in the temperature range 5–41°C and NaCl concentration range 1–50 meq l^{-1} are established. Intra-membrane frictional coefficients are linked to nanofilter morphological and charge characteristics in the context of our recent publications (Sharma *et al.* 2003; Sharma & Chellam 2005, 2006).

THEORETICAL WORK

The fluxes of pure water (J_v) and solute (J_s) are related to their respective driving forces, the trans-membrane pressure (ΔP_{TM}) and the concentration gradient (dc/dx)

(Kedem & Katchalsky 1958) as:

$$J_v = L_p \Delta P_{TM} \tag{1}$$

$$J_s = -P\Delta x\left(\frac{dc}{dx}\right) + (1-\sigma)J_v c \tag{2}$$

where, pure water permeability (L_p), solute reflection coefficient (σ) and solute diffusive permeability (P) are three phenomenological transport parameters, c is the concentration, x is the coordinate perpendicular to membrane surface, and Δx is the effective distance travelled by solutes and water across the membrane. The term $(1-\sigma)$ in Equation 2 is the coupling factor between water and solute representing convective solute transport. At steady state, substituting the solute flux as $J_v C_P$, an expression for the intrinsic rejection (R) in terms of permeate and membrane surface solute concentrations (C_p and C_m) can be obtained by integrating Equation 2 as:

$$R = 1 - \frac{C_p}{C_m} = \frac{\sigma(1-F)}{1-\sigma F} \tag{3}$$

where $F = \exp\left(-\frac{1-\sigma}{P}J_v\right)$. Next, chemical potential gradients across the membranes for water and solute transport (thermodynamic forces) were transformed to frictional forces and simplified using Onsager's reciprocal condition (Kedem & Katchalsky 1961; Ginzburg & Katchalsky 1963). Thus, the coefficients L_p, σ and P can be 'translated' to solute–membrane (F_{sm}), water–membrane (F_{wm}) and solute–water (F_{sw}) interactions (Kedem & Katchalsky 1961; Ginzburg & Katchalsky 1963):

$$F_{sw} = \left(1 - \sigma - \frac{\omega \bar{V}_s}{L_P}\right)\frac{\phi_w}{\omega \Delta x} = F^*_{sw}\frac{\phi w}{\Delta x} \tag{4}$$

$$F_{sm} = \left(\sigma + \frac{\omega \bar{V}_s}{L_P}\right)\frac{\phi_w}{\omega \Delta x} = F^*_{sm}\frac{\phi_w}{\Delta x} \tag{5}$$

$$F_{wm} = \left[\frac{1}{L_p} - \frac{(1-\sigma)\left(\sigma + \frac{\omega \bar{V}_s}{L_P}\right)\bar{C}_s}{\omega}\right]\frac{\phi_w \bar{V}_w}{\Delta x} = F^*_{wm}\frac{\phi_w}{\Delta x} \tag{6}$$

where, F_{sw}, F_{sm} and F_{wm} are the frictional coefficients for solute–water, solute–membrane and water–membrane interactions, respectively. ω (= P/RT for neutral alcohols and sugars and = P/2RT for NaCl and $NaClO_4$) is the solute permeability (Lakshminarayanaiah 1969), $\bar{V}_s$ and $\bar{V}_w$ are the partial molar volumes of the solute and water, $\bar{C}_s$ is the average of feed and permeate concentrations, and ϕ_w is the water content or porosity of the membrane. It should be noted that some reports of electrolyte frictional coefficients have omitted the factor of 2 in the denominator of ω (e.g. Szanuawska & Spencer 1994, 1997) resulting in incorrect values for the frictional coefficients. The porosity and the pore tortuosity of the active layer of thin-film composite NF membranes cannot be directly measured in the laboratory because pores are <2 nm in size (Koros *et al.* 1996). Hence, in this paper they are lumped along with the apparent frictional coefficient, F^*_{ij} (similar to Szanuawska & Spencer 1994, 1997; Yang & Liu 1998), to obtain absolute friction coefficients, F_{ij}. Note that the term $\omega \bar{V}_s/L_p$, which appears in Equations 4, 5 and 6 is analogous to an inverse Peclet number (also known as dispersion number). Under our experimental conditions, this term $\rightarrow 0$ indicating pressure-driven convection of water dominated solute diffusive permeability.

F_{wm} and F_{sm} represent interactions of one mole of water and solute, respectively, with the polymeric network constituting the NF membrane. Similarly, F_{sw} is the interaction of one mole of solute with water molecules in its vicinity within the membrane (Kaufmann & Leonard 1968). Hence, frictional coefficients are the macroscopic manifestation of all intra-membrane molecular collisions that cause deviations from a direct passage of water and solutes across the nanofilter. Importantly, frictional coefficients reported in this paper are 'effective' values associated with the entire thin-film composite membrane (including the ultrathin nanoporous active layer, microporous support layer and the reinforcing fabric). This is because solute transport across the multiple layers was analysed holistically since information on the individual layers is not available to us (deemed proprietary by the manufacturers).

σ, P and L_p were obtained by fitting Equations 1 and 3 to laboratory measurements of solute rejections and water fluxes at various pressures as described in our earlier publications (Sharma *et al.* 2003; Sharma & Chellam 2005, 2006). Molar volumes of neutral organic solutes were obtained from Hayduk & Laudie (1974) and that of electrolytes and water ($18.1\ cm^3\ mol^{-1}$) from Horvath (1985) and Marcus (1985). Apparent friction coefficients for each solute and water were calculated using the corresponding phenomenological parameters and molar volumes.

EXPERIMENTAL WORK

Because detailed information on experimental data reported in this paper including solutes and membranes employed, membrane conditioning, filtration protocols, concentration measurements, etc. have been reported by us elsewhere (Sharma *et al.* 2003; Sharma & Chellam 2005, 2006) they will not be included herein. Briefly, ACS grade ethylene glycol, t-butyl alcohol, dextrose xylose and glycerol were used because these highly soluble alcohols and sugars facilitate studies of hindered transport across membranes (Aimar *et al.* 1989; Tam & Tremblay 1991; Bowen *et al.* 1997; Sharma *et al.* 2003). Substantial (>10%) loss of t-butyl alcohol was measured in the feed tank at 41°C presumably due to volatilization. Additionally, diffusive permeabilities of xylose and dextrose $\rightarrow 0$ for both membranes at 5°C and 15°C (almost no pressure dependence on rejection). Hence, transport measurements of these solute–temperature combinations could not be included in the theoretical analysis.

Two commercially available thin-film composite membranes designated as DL (Osmonics, Minnetonka, Minnesota) and TFCS (Koch Fluid Systems, San Diego, California) by their respective manufacturers were employed. Both membranes have a proprietary polyamide skin layer supported by more than one porous sub-layer. The exact composition of functional groups comprising the skin layer was not made available to us. The TFCS membrane has smaller values of both mean pore size (0.96 nm) and molecular weight cut-off, MWCO (180 Da) when compared with DL membrane (mean pore size $= 1.44$ nm and MWCO $= 268$ Da) (Sharma *et al.* 2003; Sharma & Chellam 2005). Membrane surface charge calculations employing rejection measurements of $1\,\mathrm{meq\,l^{-1}}$ NaCl feed concentration and Donnan-Steric partitioning pore model at room temperature (23°C) under slightly acidic conditions ($\mathrm{pH} = 5.9 \pm 0.3$) revealed the TFCS membrane to be more negatively charged than the DL membrane ($-6.7\,\mathrm{meq\,l^{-1}}$ and $-1.4\,\mathrm{meq\,l^{-1}}$, respectively) (Sharma & Chellam 2006).

Five to seven different pressures in the range 100–760 kPa were employed for each solute, membrane and temperature combination. This pressure range resulted in permeate fluxes between 0.77 and $10\,\mu\mathrm{m\,s^{-1}}$ at 23°C. The system was operated at very low (<1%) recovery to minimize possible changes in bulk concentration and concentration polarization along the length. Both permeate and concentrate flow streams were recirculated to the feed tank except during sampling. The use of a spacer along with crossflow velocities of $9.6\,\mathrm{cm\,s^{-1}}$ and $19.2\,\mathrm{cm\,s^{-1}}$ (for DL and TFCS membrane, respectively) effectively eliminated concentration polarization effects in the entire range of pressures and temperatures investigated in this study (Sharma *et al.* 2003; Sharma & Chellam 2005, 2006). Hence, under our experimental conditions, frictional resistances to solute transport within the concentration boundary layer on the feed (brine) side were negligible. However, phenomenological parameters can be calculated even in the presence of a concentration polarization layer (e.g. Sharma *et al.* 2003) and used as input to the frictional model.

Experiments with dilute solutions (0.28–0.83 μM for alcohols and sugars, each corresponding to $20\,\mathrm{mg\,l^{-1}}$ total organic carbon concentration, and 1 mM for NaCl and $NaClO_4$) were performed at 5, 15, 23, 35 and 41°C. Experiments were also performed with NaCl at 1, 5, 10 and $50\,\mathrm{meq\,l^{-1}}$ to analyse concentration effects at 5, 23, 35 and 41°C. At all temperatures and concentrations evaluated, the second term in the parenthesis of Equation 6 was negligible compared with the first term ($1/L_p$), demonstrating that solute contributions to water–membrane interactions could be neglected. Solute–solute interactions were also insignificant under experimental conditions reported in this paper. Therefore, frictional coefficient between the solute and water in the bulk solution was calculated using the expression for dilute binary systems (Cussler 1984):

$$F_{sw}^{0} = \frac{RT}{D_{\infty}} \tag{7}$$

Experimentally measured bulk diffusion coefficients, D_∞, at 25°C (Washburn 1929; Hayduk & Laudie 1974; Wang *et al.* 1995*a*) were used to calculate the effective hydrodynamic radius using the Stokes-Einstein equation.

RESULTS AND DISCUSSION

Brief statement of experimental reproducibility

Selected experiments with ultrapure water, sugars, alcohols and electrolytes were repeated to examine possible changes

in their rejection by the membrane coupons employed over the entire duration of experimentation. Extremely similar profiles for water flux and solute rejection with transmembrane pressure were obtained for duplicate experiments, which revealed no statistical differences (at 0.05 significance level) in all phenomenological parameters, L_p, σ and P. Hence, data obtained during the two years of laboratory work could be quantitatively analysed. A comprehensive discussion of our quality control and quality assurance protocols and results can be found elsewhere (Sharma *et al.* 2003; Sharma & Chellam 2005, 2006).

Calculations of phenomenological parameters

In this section, two fluxes (water and solute) have been analysed using three phenomenological coefficients (L_p, P, σ). Figure 1(a) summarizes the dependence of water flux on transmembrane pressure for the DL membrane. As observed, water flux increased linearly at all temperatures ($R^2 > 0.99$) indicating that membrane fouling and compaction were negligible, allowing the estimation of L_p as the slope of straight-lines fits to experimental data (see Equation 1). As can be expected simply from considerations of viscosity, L_p values for the DL membrane in Figure 1 increased with temperature (higher slopes). Similar results were obtained for the TFCS membrane.

Solute reflection coefficients and diffusive permeabilities were calculated using non-linear regression by employing Equation 3 and solute rejection measurements over a wide range of pressures (fluxes) at very low recoveries and high crossflow velocities. The sum of squares of the error for all experimental data points was minimized using the Solver tool in Microsoft Excel with 5% tolerance and 10^{-6} precision to determine σ and P. Mathematically from Equations 1 and 3, as $\Delta P \rightarrow \infty$, $J_v \rightarrow \infty$ and $R \rightarrow \sigma$. Hence, experimental solute rejection for the DL membrane was plotted as a function of inverse permeate flux in Figure 1(b) wherein the solid line corresponds to best-fits of Equation 3. The y-axis intercept corresponds to σ and P is a measure of the curvature of the rejection profile. It is important to note that in the absence of solute–water coupling and concentration polarization, solutes will be perfectly rejected at very high flux ($\sigma = 1$ independent of solute size) based on purely solution-diffusion arguments. In contrast, $0 < \sigma < 1$ for various solutes employed in this study indicating strong coupling between solute and water transport signifying the porous nature of the DL membrane. Further, consistent with the theory of hindered transport across porous membranes, σ increased with solute size. Increased coupling between solute and water $(1 - \sigma)$ with decreasing solute size further validates usage of porous membrane analogy for the DL membrane.

Similar results were obtained for electrolytes and the TFCS membrane for all temperatures investigated. Hence, convective pore flow was an important transport mechanism for both DL and TFCS membranes. Substantially more

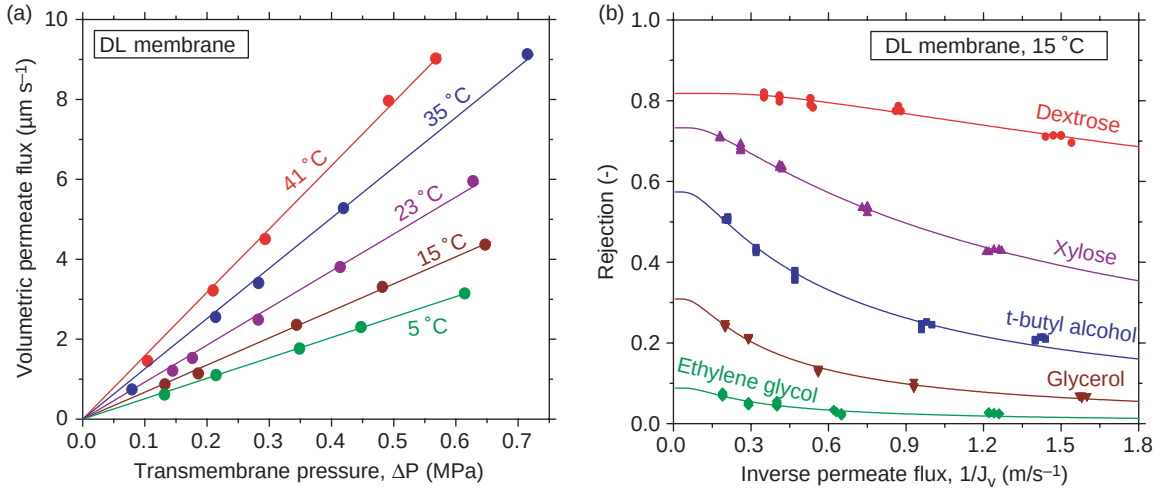

Figure 1 | Experimental measurements of DL membrane–neutral solutes phenomenological parameters. Pure water permeabilities at various temperatures are depicted in (a). Neutral solutes reflection coefficients and diffusive permeabilities are estimated from (b).

information on the fitting procedure and temperature and concentration effects on laboratory rejection profiles can be obtained from our recent publications (Sharma *et al.* 2003; Sharma & Chellam 2005, 2006). Phenomenological parameters L_p, σ and P for both membranes were 'translated' into apparent frictional coefficients F^*_{wm}, F^*_{sm}, *and* F^*_{sw} using Equations 4, 5 and 6 as described next.

Friction coefficients of neutral solutes at any given temperature

Apparent friction coefficients of alcohols and sugars at all temperatures investigated are given in Tables 1 and 2 for the DL and TFCS membranes, respectively. Room temperature results are summarized in Figure 2. Several observations can be made from Tables 1 and 2 and Figure 2. First, water–membrane friction coefficients were 2–5 orders of magnitude smaller than apparent solute–membrane friction coefficients, demonstrating that nanofilters hindered solutes to a substantially greater degree than water (prerequisite for contaminant rejection).

Second, apparent frictional interactions increased with solute size. Third, stronger apparent solute–membrane interactions were obtained for the 'tighter' TFCS membrane compared with the 'looser' DL membrane. In other words, higher F^*_{sm} values were calculated for the TFCS membrane because it had a lower average pore size (0.96 nm at 23°C) compared with the DL membrane (1.44 nm at 23°C) (Sharma *et al.* 2003; Sharma & Chellam 2005). Even though frictional coefficients are not amenable to detailed mechanistic interpretations, similar trends are predicted by purely hydrodynamic simulations of solute transport across straight slit or cylindrical pores with fully developed flow (Deen 1987). Fourth, non-zero F^*_{sw} values indicate that water and solute molecules followed the same path within the polymeric matrix of the NF membrane, resulting in substantial coupling between them. Importantly, this is a prerequisite for a porous membrane, justifying our earlier use of the Donnan steric partitioning pore model to quantify salt and neutral solute rejection by the DL and TFCS membranes (Sharma & Chellam 2005, 2006). Note that for a perfect reverse osmosis membrane F^*_{sw} will be equal to zero because, according to the solution–diffusion model (Wijmans & Baker 1995), water and solutes permeate independently through different pathways.

Fifth, as seen in Tables 1 and 2 the F_{sw}/F_{sm} ratio was typically <1 demonstrating that solute–membrane interactions controlled neutral solute rejection for both the membranes. (Note that the ratio of porosity to membrane thickness cancels in the numerator and denominator allowing a discussion of the absolute friction coefficients ratio.) Sixth, the F_{sw}/F_{sm} ratio increased with decreasing solute size for both membranes. Decreasing solute size reduces both F^*_{sw} and F^*_{sm} even in cylindrical pores due to lower hydrodynamic drag. However, we have recently shown that both membranes exhibit highly solute-dependent tortuosities (Sharma & Chellam 2005). In other words, smaller solutes traverse a longer path within the water-filled pores of both membranes, not decreasing F^*_{sw} as much as in a perfectly cylindrical pore. Hence, the rate of decrease of the numerator (F^*_{sw}) is lower compared with the rate of decrease of the denominator (F^*_{sm}), together increasing the F_{sw}/F_{sm} ratio. These are the first reports of increasing F_{sw}/F_{sm} ratios with decreasing solute size for pressure-driven nanofilters even though such a behaviour has been observed in biological and dialysis systems (Ginzburg & Katchalsky 1963; Kaufmann & Leonard 1968; Kokubo & Sakai 1998).

Additionally, this effect is highest for the smallest solutes (ethylene glycol, glycerol and t-butyl alcohol for the DL membrane and ethylene glycol for the TFCS membrane), wherein the F_{sw}/F_{sm} ratio was even increased beyond unity. The cumulative effects of membrane porosity and solute effective tortuosity (Sharma & Chellam 2005) cause F^*_{sw} to even supersede F^*_{sm} for these solute–membrane combinations.

Next, as proposed earlier (Kaufmann & Leonard 1968), normalized solute–membrane and solute–water friction coefficients at each temperature T were calculated by normalizing the absolute friction with that of the smallest molecule employed, namely, ethylene glycol:

$$\left(F^*_{sm}\right)_{i,T} = \frac{(F_{sm})_{i,T}}{(F_{sm})_{ethylene\,glycol,\,T}} \tag{8}$$

$$\left(F^*_{sw}\right)_{i,T} = \frac{\left(F^0_{sw}/F_{sw}\right)_{i,T}}{\left(F^0_{sw}/F_{sw}\right)_{ethylene\,glycol,\,T}} \tag{9}$$

Normalized friction coefficients were negatively correlated for both thin-film composite nanofilters in this study as

Table 1 | Apparent frictional coefficients (N-s mol$^{-1} \times 10^{-8}$) and activation energies for neutral solute permeation across the DL membrane

Solute	Stokes radius (nm)	Temp (°C)	F°_{sw}	F°_{sm}	$F^{\circ}_{sw}/F^{\circ}_{sm}$	F°_{wm}	E°_{sw} (kJ mol^{-1})	F°_{sm} (kJ mol^{-1})
Dextrose	0.366	5	37.9	251.5	0.15	0.035	39.1 ± 7.0	56.0 ± 3.6
		15	28.4	129.0	0.22	0.026		
		23	22.3	73.9	0.30	0.019		
		35	7.3	23.8	0.31	0.014		
		41	6.4	17.1	0.37	0.011		
Xylose	0.300	5	13.8	53.2	0.26	0.035	19.8 ± 2.7	47.7 ± 0.7
		15	9.4	26.6	0.35	0.026		
		23	7.5	14.7	0.51	0.019		
		35	5.1	7.1	0.72	0.014		
		41	5.5	5.1	1.08	0.011		
t − butyl alcohol	0.278	5	10.1	21.7	0.46	0.035	22.3 ± 4.5	57.8 ± 1.9
		15	7.2	9.1	0.79	0.026		
		23	4.8	4.4	1.08	0.019		
		35	4.1	1.9	2.13	0.014		
Glycerol	0.258	5	5.4	4.3	1.26	0.035	4.5 ± 1.4	32.2 ± 1.4
		15	5.9	2.8	2.10	0.026		
		23	5.9	1.8	3.35	0.019		
		35	4.6	1.1	4.16	0.014		
		41	4.6	0.9	5.16	0.011		
Ethylene glycol	0.211	5	7.1	1.1	6.32	0.035	2.9 ± 1.3	20.9 ± 2.8
		15	6.4	0.7	8.86	0.026		
		23	6.0	0.7	8.57	0.019		
		35	6.3	0.5	13.25	0.014		
		41	6.0	0.4	16.23	0.011		

Note: $F^{\circ}_{sw}/F^{\circ}_{sm}$ is identical to F_{sw}/F_{sm} since the ratio of porosity to membrane thickness cancels from the numerator and the denominator. $E^{\circ}_{wm} = 24.1 \pm 0.9$ kJ/mol.

shown in Figure 3 and reported earlier for a regenerated cellulose acetate membrane (Kaufmann & Leonard 1968). Analysis of previously reported friction coefficients for other cellulosic membranes (Ginzburg & Katchalsky 1963) also revealed a similar trend (data not shown). This again underscores the fact that smaller solutes effectively traversed a longer path to permeate across the membranes (i.e. higher tortuosity; Kokubo & Sakai 1998; Sharma &

Table 2 | Apparent frictional coefficients (N-s mol^{-1} × 10^{-8}) and activation energies for neutral solute permeation across the TFCS membrane

Solute	Stokes radius (nm)	Temp (°C)	F^*_{sw}	F^*_{sm}	F^*_{sw}/F^*_{sm}	F^*_{wm}	E^*_{sw} (kJ mol^{-1})	E^*_{sm} (kJ mol^{-1})
Dextrose	0.366	23	34.3	211.8	0.16	0.015	30.7 ± 24.0	51.1 ± 41.5
		35	28.9	139.5	0.21	0.011		
		41	15.7	60.1	0.26	0.009		
Xylose	0.300	23	19.3	95.1	0.20	0.015	29.7 ± 6.3	41.9 ± 19.6
		35	12.8	59.3	0.22	0.011		
		41	9.8	35.7	0.28	0.009		
t − butyl alcohol	0.278	5	12.3	29.7	0.42	0.026	18.6 ± 4.6	19.8 ± 9.8
		15	12.2	19.4	0.63	0.019		
		23	6.1	19.5	0.31	0.015		
		35	6.1	12.8	0.47	0.011		
Glycerol	0.258	5	6.8	10.8	0.63	0.026	7.5 ± 1.8	19.5 ± 5.3
		15	6.7	10.2	0.66	0.019		
		23	6.0	9.5	0.63	0.015		
		35	5.6	5.0	1.12	0.011		
		41	4.7	4.6	1.02	0.009		
Ethylene glycol	0.211	5	3.2	1.6	1.97	0.026	14.8 ± 2.0	24.3 ± 1.7
		15	2.4	1.0	2.31	0.019		
		23	2.0	0.9	2.22	0.015		
		35	1.6	0.6	2.78	0.011		
		41	1.6	0.5	3.28	0.009		

Note: F^*_{sw}/F^*_{sm} is identical to F_{sw}/F_{sm} since the ratio of porosity to membrane thickness cancels from the numerator and the denominator. $E^*_{wm} = 21.8 \pm 0.5$ kJ/mol.

Chellam 2005) increasing solute–water interactions (higher F^*_{sw}). Simultaneously, smaller solutes experience reduced steric interactions with the membrane (lower F^*_{sm}).

Temperature effects on neutral solutes friction coefficients

All friction coefficients were inversely related to temperature analogous to water viscosity. Figure 4 depicts temperature effects on the ratio of the total friction to water transport ($F_w = F_{wm} + F_{sw}$) to the total friction to solute transport ($F_s = F_{sm} + F_{sw}$). Note that F_s is the total interaction of 1 mole of solute with the polymeric membrane matrix and pore water in its vicinity. F_w/F_s is proportional to $(1 - \sigma)$, which is equivalent to solute passage at asymptotically infinite flux, which can also be interpreted as the ratio of solute velocity to water velocity in the pore.

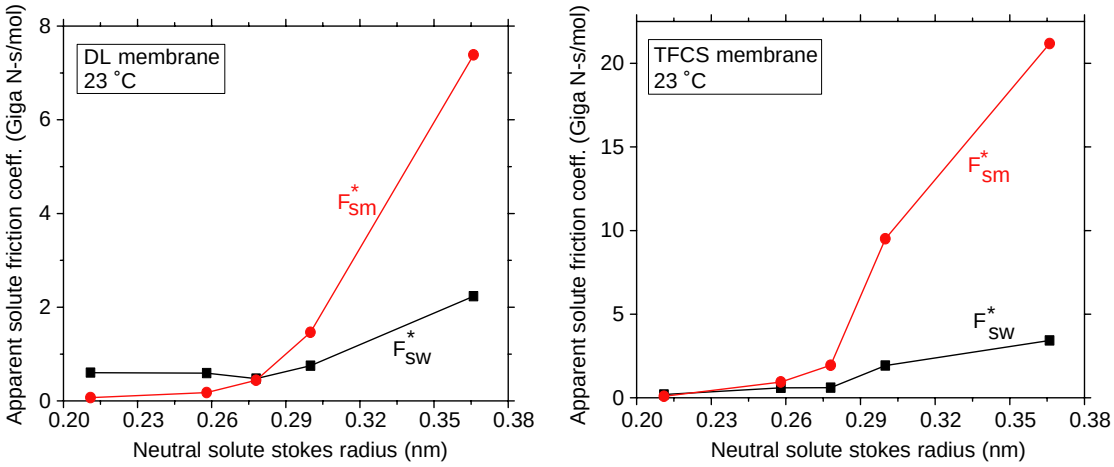

Figure 2 | Friction coefficients for neutral solute–membrane and neutral solute–water interactions for both membranes at room temperature.

As observed, these ratios: (1) were always <1 demonstrating the semi-permeable nature of these membranes; (2) decreased as solute size increased due to steric effects on membrane selectivity; and (3) increased with temperature suggesting that warmer feed waters have a greater influence on solute velocity than water velocity. Differences in the rate of change of solute and water velocities with temperature indicate temperature-induced morphological changes in the nanofilter, which serves as the barrier between the feed water and the permeate water. Conceptually, this is similar to rate constants varying with temperature for chemical reactions, quantified as activation energies.

Activation energies (E_{ij}^{*}) for the apparent friction coefficients (F_{ij}^{*}) were calculated from semi-log fits of F_{ij}^{*} as a function of 1/T as suggested by the Arrhenius equation:

$$F_{ij}^{*} = A\exp\left(\frac{E_{ij}^{*}}{RT}\right) \tag{10}$$

and are also given in Tables 1 and 2. The negative sign usually employed in the exponential term of Equation 10 has been removed analogous to activation energy calculations of viscosity (Barrer 1942), because frictional interactions also decreased with temperature. The mean value and standard deviation of the slope (which corresponds to E_{ij}^{*}/R) were estimated using linear regression. Thus, activation energies reported in this paper represent an average value valid in the temperature range 5–41°C. In all cases, $E_{sw}^{*} < E_{sm}^{*}$ demonstrating that increasing temperature reduced F_{sm}^{*} at a greater rate than F_{sw}^{*}. This resulted in the increasing F_{sw}/F_{sm} ratio for all solutes with temperature for both membranes. Hence, the relative importance of solute–membrane interactions (compared with solute–water interactions) decreased with temperature. Mechanistically, this is consistent with our recent results (Sharma *et al.* 2003; Sharma & Chellam 2005), where pathways for solute passage within the polymeric membrane opened up with increasing temperature. In other words, solutes are able to pass through more easily for warmer feed waters because their interactions with the polymeric membrane matrix are reduced.

Also as seen in Tables 1 and 2, E_{sm}^{*} and E_{sw}^{*} generally increased with solute size as a result of membranes

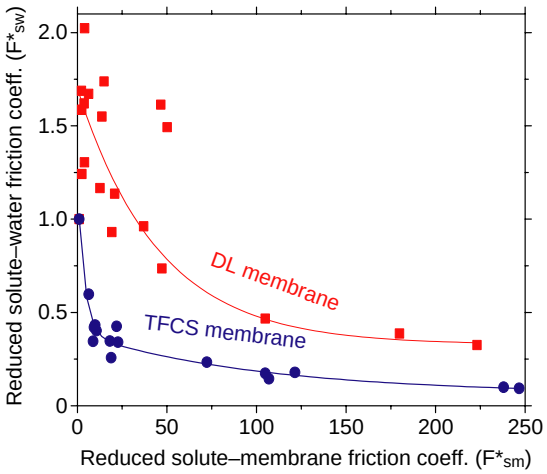

Figure 3 | Interdependence of reduced friction coefficients for both thin-film composite nanofilters.

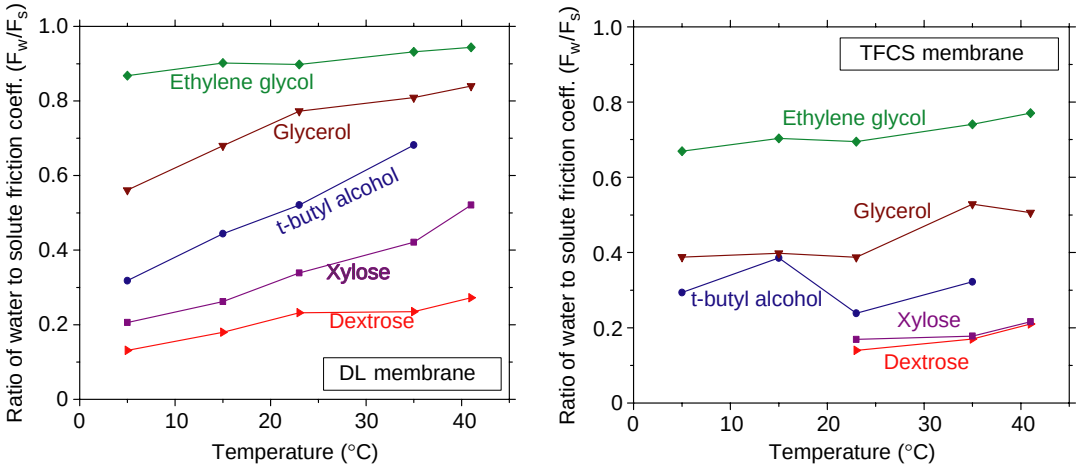

Figure 4 | Temperature effects on the ratio of the total friction to water transport to the total friction to solute transport for both membranes.

presenting greater hindrances to the passage of larger solutes (Sharma *et al.* 2003), which can be interpreted in terms of the free volume theory of diffusive transport (Kumins & Kwei 1968). Sufficient thermal energy becomes available to form larger 'holes' or 'voids' in the water or the polymer matrix as feed water temperature increases. Jump probability for larger solutes increases with temperature since they can now effectively occupy the larger voids allowing their easier passage across the membrane. The activation energies of small solutes are smaller because formation of larger voids does not influence their jump probability. E^{*}_{wm} remained constant for each membrane denoting that it was independent of the presence of solute validating the neglect of solute–solute interactions in this paper (dilute solutions).

Equivalence of hydrodynamic and phenomenological approaches for neutral solutes

Hydrodynamic arguments wherein typically spherical solutes are assumed to be moving in a fully developed flow-field within cylindrical pores are popular in interpreting neutral solute passage across porous NF and UF membranes (Malone & Anderson 1978; Deen 1987; Mochizuki & Zydney 1993; Sharma & Chellam 2005). The advantage of using frictional coefficients to perform similar interpretations is that idealizations regarding solute and pore geometries are not required. Possible relationships between these two approaches were explored by first comparing the ratio of solute interactions in the bulk solution (F^{0}_{sw}) to that within the nanoporous membrane ($F_{sm}+F_{sw}$) for the case of a sphere moving in a stationary liquid (Nakao 1986):

$$\frac{F^{0}_{sw}}{F_{sw}+F_{sm}}=\frac{1}{f(q)}=\frac{1-0.75857q^{5}}{1-2.105q+2.0865q^{3}-1.7068q^{5}+0.72603q^{6}} \quad (11)$$

where q is the ratio of solute to pore radius and $f(q)$ is a diffusive wall correction factor within the pore. A similar ratio for a stationary sphere in a moving liquid was also employed (Nakao 1986):

$$\frac{F^{0}_{sw}}{F_{sw}}=\frac{f(q)}{g(q)}=\frac{1-2.105q+2.0865q^{3}-1.7068q^{5}+0.72603q^{6}}{1-0.6667q^{2}-0.20217q^{5}} \quad (12)$$

where $g(q)$ is a wall correction factor for filtration. Note that apparent friction coefficients obtained in this study (from Tables 1 and 2) were multiplied by our recent calculations of the ratio of porosity to solute path length to obtain the absolute friction coefficients in Equations 11 and 12 as required by Equations 4 and 5.

Experimental friction coefficients normalized according to the left hand side of Equations 11 and 12 are superposed on theoretical calculations according to the right hand side

of Equations 11 and 12 in Figure 5. Note that these comparisons have been made in a completely predictive mode involving no fitting of models to experimental data. Average pore sizes calculated for the DL and TFCS membranes (Sharma & Chellam 2005) have been used to normalize solute sizes to obtain the appropriate abscissa for experimental data. Figure 5 indicates that hydrodynamic arguments can be quantitatively made to interpret friction coefficients of neutral solutes in composite NF membranes because: (1) the same trends between experimental data and purely predictive calculations can be observed; and (2) a similar level of agreement was obtained compared with track-etched microfilters and ultrafilters (Malone & Anderson 1978; Deen 1987). Greater drag inside pores compared with the unbounded fluid resulted in both the frictional coefficient ratios being < 1. Additionally, as expected from theory (Equations 11 and 12), experimental friction coefficient ratios at all temperatures overlapped on the same curve in Figure 5 confirming the validity of hydrodynamic hindered transport theories to interpret neutral solute friction coefficient results.

Electrolyte frictional coefficients

Lumped NaCl and $NaClO_4$ friction coefficients at all temperatures investigated are given in Table 3 for both the DL and TFCS membranes, from which several observations can be made. First, similar to neutral solutes, apparent water–membrane friction coefficients were orders of magnitude smaller (2–3) than salt friction coefficients. Second, apparent salt–membrane friction coefficients were higher for the TFCS membrane because it was more highly charged (Sharma & Chellam 2006) and had a smaller average pore size (Sharma *et al.* 2003; Sharma & Chellam 2005) than the DL membrane. Higher electrostatic and steric interactions in the TFCS membrane reduced the relative importance of salt–water interactions by increasing solute–membrane interactions (lower F_{sw}/F_{sm} ratio). Also similar to neutral solutes, F^*_{sw} and F^*_{sm} increased with effective electrolyte Stokes radius (0.136 nm for NaCl and 0.143 for $NaClO_4$) again underscoring the importance of both steric and electrostatic interactions for 1-1 electrolyte rejection by these membranes.

Temperature and concentration effects on electrolyte frictional coefficients

Similar to neutral sugars and alcohols, increasing temperature reduced F^*_{sw}, F^*_{sm} and F^*_{wm} for both membranes (see Table 3). However, temperature had opposite effects on F_{sw}/F_{sm} ratios for electrolytes and neutral organic solutes. Electrolyte F_{sw}/F_{sm} ratios were negligibly impacted for the TFCS membrane and even decreased for the DL membrane with temperature. These trends for electrolytes and neutral solutes are the net effects of (1) reduced water viscosity, (2) opening up of the nanofilters' polymeric matrix (Sharma *et al.* 2003; Sharma & Chellam 2005), and (3) higher charge density (Sharma & Chellam 2006) for

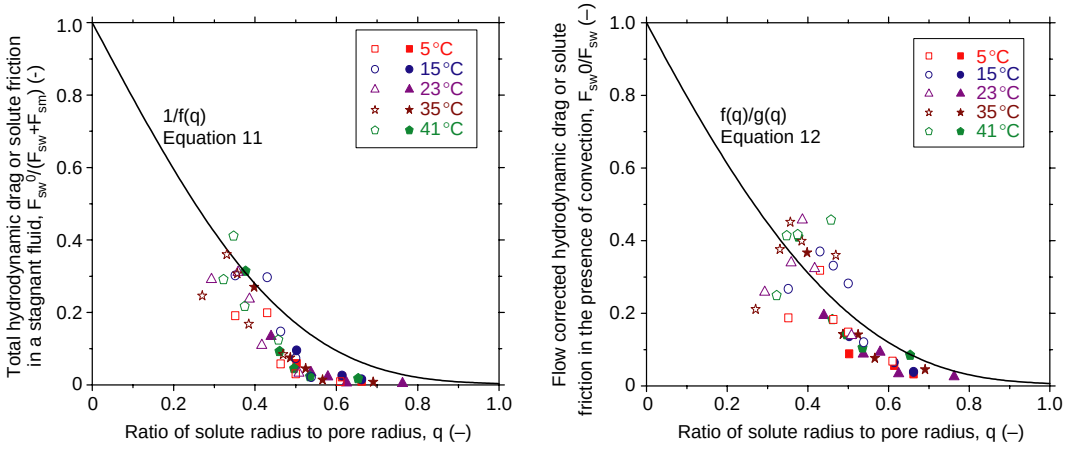

Figure 5 | Comparison of frictional coefficient ratios with hydrodynamic models of hindered transport. Open symbols represent DL membrane data and filled symbols correspond to the TFCS membrane.

Table 3 | Apparent frictional coefficients (N-s mol^{-1} × 10^{-8}) and activation energies for 1:1 electrolyte permeation across both membranes (concentration = 1 meq l^{-1})

Membrane	Solute	Temp (°C)	F^*_{sw}	F^*_{sm}	F^*_{sw}/F^*_{sm}	F^*_{wm}	E^*_{sw} (kJ mol^{-1})	E^*_{sm} (kJ mol^{-1})	E^*_{wm} (kJ mol^{-1})
TFCS	NaCl	5	28.0	130.4	0.21	0.026	14.8 ± 1.7	13.4 ± 1.9	21.8 ± 0.5
		15	22.4	106.8	0.21	0.019			
		23	20.1	87.2	0.23	0.015			
		35	14.4	69.8	0.21	0.011			
		41	14.3	72.0	0.20	0.009			
	$NaClO_4$	5	42.6	193.6	0.22	0.026	13.9 ± 4.1	16.1 ± 4.4	
		15	28.3	127.8	0.22	0.019			
		23	25.4	105.0	0.24	0.015			
		35	20.1	83.0	0.24	0.011			
		41	22.0	91.8	0.24	0.009			
DL	NaCl	5	35.9	45.3	0.79	0.035	19.6 ± 1.6	11.3 ± 3.3	24.1 ± 0.9
		15	27.2	32.7	0.83	0.026			
		23	21.1	27.3	0.77	0.019			
		35	14.8	26.8	0.55	0.014			
		41	14.4	24.8	0.58	0.011			
	$NaClO_4$	5	49.4	60.2	0.82	0.035	22.7 ± 1.7	14.1 ± 2.0	
		15	38.0	43.0	0.88	0.026			
		23	26.2	36.7	0.72	0.019			
		35	17.5	31.0	0.56	0.014			
		41	17.8	29.4	0.61	0.011			

Note: F^*_{sw}/F^*_{sm} is identical to F_{sw}/F_{sm} since the ratio of porosity to membrane thickness cancels from the numerator and the denominator.

warmer feed waters. Reduced water viscosity and higher pore size will reduce both F_{sw} and F_{sm}. However, increasing charge densities with temperature for the two membranes employed in this study partially compensated for purely viscous and steric contributions to F^*_{sw} and F^*_{sm} resulting in different trends between electrolytes and neutral compounds. Even though our observations have been made using idealized single salt solutions, they can partially explain temperature effects on ion and conductivity rejection from natural waters by polymeric NF and RO membranes (Ventresque *et al.* 1997; Taniguchi & Kimura 2000).

Different mean pore sizes, permeation pathways, and charge densities at any given temperature for the DL and TFCS membranes coupled to their different responses to temperature variations disallow a simple explanation for the observed differences in the F_{sw}/F_{sm} trends for NaCl and $NaClO_4$ summarized in Table 3.

Table 4 | Concentration and temperature dependence of NaCl apparent frictional coefficients (N-s mol^{-1} × 10^{-8}) and activation energies

Membrane	Concentration	Temp (°C)	F^*_{sw}	F^*_{sm}	F^*_{sw}/F^*_{sm}	F^*_{wm}	E^*_{sw} (kJ mol^{-1})	E^*_{sm} (kJ mol^{-1})	E^*_{wm} (kJ mol^{-1})
TFCS	1	5	28.0	130.4	0.21	0.026	14.8 ± 1.7	13.4 ± 1.9	21.8 ± 0.5
		23	20.1	87.1	0.23	0.015			
		35	14.4	69.8	0.21	0.011			
		41	14.3	72.0	0.20	0.009			
	5	5	20.9	61.4	0.34	0.026	19.1 ± 4.5	11.7 ± 4.4	
		23	12.1	42.1	0.29	0.015			
		35	8.3	32.9	0.25	0.011			
		41	9.3	38.4	0.24	0.009			
	10	5	21.0	45.8	0.46	0.026	19.9 ± 2.6	11.9 ± 2.0	
		23	13.5	34.4	0.39	0.015			
		35	9.0	27.0	0.33	0.011			
		41	8.7	27.3	0.32	0.009			
	50	5	7.0	17.1	0.41	0.026	28.6 ± 1.1	10.4 ± 2.1	
		23	3.3	14.2	0.23	0.015			
		35	2.4	11.0	0.22	0.011			
		41	1.8	10.8	0.16	0.009			
DL	1	5	35.9	45.3	0.79	0.035	19.6 ± 1.6	11.3 ± 3.3	24.1 ± 0.9
		23	21.1	27.3	0.77	0.019			
		35	14.8	26.8	0.55	0.014			
		41	14.4	24.8	0.58	0.011			
	5	5	28.3	10.2	2.76	0.035	27.9 ± 9.7	8.8 ± 5.2	
		23	9.2	6.4	1.43	0.019			
		35	6.7	6.3	1.06	0.014			
		41	8.5	7.1	1.20	0.011			
	10	5	29.1	5.7	5.10	0.035	29.3 ± 5.6	7.9 ± 1.9	
		23	10.0	4.3	2.34	0.019			
		35	7.7	3.9	1.98	0.014			
		41	7.4	4.0	1.85	0.011			
	50	5	22.8	2.0	11.63	0.035	27.1 ± 2.8	7.9 ± 2.6	
		23	9.9	1.8	5.57	0.019			
		35	6.8	1.4	4.92	0.014			
		41	6.6	1.4	4.78	0.011			

Note: F^*_{sw}/F^*_{sm} is identical to F_{sw}/F_{sm} since the ratio of porosity to membrane thickness cancels from the numerator and the denominator.

Invariant F_{sw}/F_{sm} ratios resulted in comparable electrolyte activation energies E^*_{sw} and E^*_{sm} for the TFCS membrane because temperature influenced solute–water and solute–membrane interactions in a similar fashion. On the other hand, $E^*_{sw} > E^*_{sm}$ for the DL membrane suggesting solute–water interactions changed to a greater degree than solute–membrane interactions as temperature changed. This is caused by simultaneous increases in pore sizes (lower steric contribution to F^*_{sm}) and charge densities (higher electrostatic contribution to F^*_{sm}) for these membranes as feed waters increased in temperature (Sharma & Chellam 2006).

Table 4 summarizes concentration effects on NaCl apparent friction coefficients for both membranes in the range 5–41°C. At any given temperature, NaCl rejection decreased at higher concentrations, which is a typical trend for charged membranes (Xu & Lebrun 1999). This can be interpreted in terms of decreasing F^*_{sm} due to increased shielding of membrane surface charges at higher ionic strengths. Even though both increasing and decreasing trends in F_{sw} have been reported in the literature (Meares *et al.* 1972), in our system F^*_{sw} consistently decreased with feed concentration for both membranes. For the DL membrane, electrostatic interactions were shielded so effectively at NaCl concentrations $>1\,\text{meq}\,\text{l}^{-1}$ that $F^*_{sm} < F^*_{sw}$. Under these conditions, solute–water interactions controlled NaCl permeation across this membrane $\left(F^*_{sw}/F^*_{sm} > 1\right)$.

Similar to neutral solutes, the ratio of the total friction to water transport $\left(F^*_w = F^*_{wm} + F^*_{sw}\right)$ to the total friction to NaCl transport $\left(F^*_s = F^*_{sm} + F^*_{sw}\right)$ was also calculated. Figure 6 depicts this ratio at different concentrations and temperatures. F_w/F_s increased monotonically with concentration for the DL membrane as a result of decreasing F^*_{sm} and F^*_{sw} due to reductions in electrostatic interactions arising from lower Donnan potentials (Sharma & Chellam 2006). Charge reversal in the TFCS membrane at $50\,\text{meq}\,\text{l}^{-1}$ caused the corresponding decrease in F^*_w/F^*_s.

For both membranes, at any given NaCl concentration F_w/F_s decreased with temperature, which is an opposite trend compared with that of neutral solutes (Figure 3). Hence, warmer feed waters increased water velocity (lower F^*_w) more than electrolyte velocity (higher F^*_s) causing the observed trends in F_w/F_s. In other words, higher feed water temperatures increased charge density thereby restricting NaCl transport while simultaneously increasing pore size facilitating water transport. Also, at a fixed concentration, F_{sw}/F_{sm} decreased with temperature (Table 4) demonstrating that the increased relative importance of solute–membrane interactions on NaCl permeation for warmer feed waters was caused by higher charge densities (Sharma & Chellam 2006).

Table 4 also shows that NaCl–membrane activation energies decreased with concentration presumably due to increased shielding of electrostatic interactions at elevated concentrations. Further, in contrast with permeation of

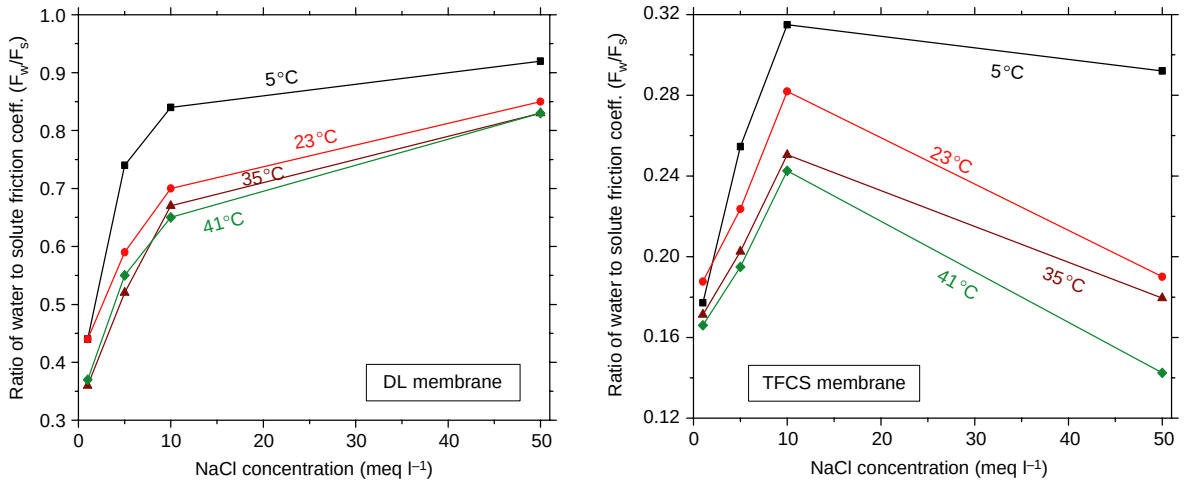

Figure 6 | Effects of concentration and temperature on F_w/F_s for NaCl.

neutral alcohols and sugars, the influence of solute–water interactions on electrolyte permeation increased with feed water temperature ($E^*_{sw} > E^*_{sm}$). E^*_{wm} was independent of concentration for both membranes demonstrating negligible modifications to the nanofilter morphology within 1–50 meq l^{-1} range considered in this paper (dilute solutions). Further, morphology of membranes did not vary with solute type (neutral solutes or electrolytes) because the same value of E^*_{wm} was obtained for all experiments.

SUMMARY AND CONCLUSIONS

Results presented in this paper follow the broad theme of our recent investigations to elucidate temperature and concentration effects on permselectivity of polymeric thin-film composite NF membranes (Sharma *et al.* 2003; Sharma & Chellam 2005, 2006) to eventually develop a rigorous understanding of seasonal effects on contaminant removal. The frictional approach was shown to be able to quantitatively simulate rejections from synthetic waters in the temperature range 5–41°C and with varying NaCl concentration in the range 1–50 meq l^{-1}. Results from this study are consistent with polymeric membranes undergoing structural and morphological changes with temperature. Consistently increasing neutral solutes permeate concentrations with temperature demonstrated that temperature had a greater effect on velocity of non-interacting solutes compared with water. Thus, for neutral solutes, $E^*_{sm} > E^*_{wm}$ and E^*_{sw}. Importantly, both E^*_{sm} and E^*_{sw} increased with solute size, as predicted from hindered transport theories.

However, ion permeation dependence on temperature is further complicated by changes in electrostatic interactions with the membrane. Increases in electrolyte permeation with temperature were observed to be much weaker compared with neutral solutes and in some cases ion permeate concentrations even decreased with temperature demonstrating opposing effects of electrostatic and steric interactions. Hence, electrolyte velocities were only weakly dependent on temperature (probably due to binding to the membrane) and simultaneous increases in water velocity increased rejection (dilution effect). Thus, in contrast to neutral solute, activation energies for electrolyte permeation were E^*_{wm} and $E^*_{sw} > E^*_{sm}$.

Reported changes in hardness (Schaep *et al.* 1998), arsenic (Waypa *et al.* 1997), natural organic matter (Her *et al.* 2000) and salts (Mehdizadeh *et al.* 1989; Ventresque *et al.* 1997; Taniguchi & Kimura 2000) removal with season and temperature can be partially explained in terms of changing intra-membrane frictional coefficients. However, it should be cautioned that the frictional model does not provide information on the effects of membrane characteristics including charge, pore shape, pore, size (distribution), tortuosity and polarity. Hence, decisions to engineer membrane properties to increase contaminant rejection cannot be made. Further, universalization or generalization of results to predict membrane rejection based on solute characteristics such as size, charge or polarity is also not possible from this approach.

ACKNOWLEDGEMENTS

David Paulson and Peter Eriksson of Osmonics Inc. and Randolph Truby and Tom Stocker of Koch Membrane Systems Inc. generously donated membrane samples. We appreciate discussions with Dr Mark Wiesner regarding frictional interpretation of solute removal. The detailed comments of three anonymous reviewers on an earlier draft of this manuscript are also appreciated. This research has been funded by a grant from the National Science Foundation CAREER program (BES-0134301). The contents do not necessarily reflect the views and policies of the sponsors nor does the mention of trade names or commercial products constitute endorsement or recommendation for use.

REFERENCES

Abdel-Jawad, M., El-Sayed, E. E. F., Ebrahim, S., Al-Saffar, A., Safar, M., Tabtaei, M. & Al-Nuwaibit, G. 2001 Fifteen years of R&D Program in Sea Water Desalination at KISR Part II. RO system performance. *Desalination* **135**, 155–167.

Aimar, P., Howell, J. A. & Turner, M. 1989 Effects of concentration boundary layer development on the flux limitations in ultrafiltration. *Chem. Eng. Res. Des.* **67**, 255–261.

Barrer, R. M. 1942 Permeability in relation to viscosity and structure of rubber. *Trans. Faraday Soc.* **38**, 322–330.

Bowen, R. W., Mohammad, A. W. & Hilal, N. 1997 Characterization of nanofiltration membranes for predictive purposes: Use of salts, uncharged solutes and atomic force microscopy. *J. Membr. Sci.* **126**, 91–105.

Bowen, W. R. & Mukhtar, H. 1996 Characterization and prediction of separation performance of nanofiltration membranes. *J. Membr. Sci.* **112**, 263–274.

Chellam, S., Jacangelo, J. G., Bonacquisti, T. P. & Schauer, B. A. 1997 Effect of pretreatment on surface water nanofiltration. *J. Am. Wat. Wks Assoc.* **89**, 77–89.

Combe, C., Molis, E., Lucas, P., Riley, R. & Clark, M. M. 1999 The effect of CA membrane properties on adsorptive fouling by humic acid. *J. Membr. Sci.* **154**, 73–87.

Cussler, E. L. 1984 *Diffusion: Mass Transfer in Fluid Systems*. Cambridge University Press, Cambridge, UK.

Deen, W. M. 1987 Hindered transport of large molecules in liquid-filled pores. *AIChE J.* **33**, 1409–1424.

Dresner, L. 1972 Some remarks on the integration of the extended Nernst-Planck equations in the hyperfiltration of multicomponent solutions. *Desalination* **10**, 27.

Ginzburg, B. Z. & Katchalsky, A. 1963 The friction coefficients of the flows of non-electrolytes through artificial membranes. *J. Gen. Physiol.* **47**, 403–418.

Hayduk, W. & Laudie, H. 1974 Prediction of diffusion coefficients for non-electrolytes in dilute aqueous solutions. *AIChE J.* **20**, 611–615.

Her, N., Amy, G. & Jarusutthirak, C. 2000 Seasonal variations of nanofiltration (NF) foulants: Identification and control. *Desalination* **132**, 143–160.

Horvath, A. L. 1985 *Handbook of Aqueous Electrolyte Solutions: Physical Properties, Estimation, and Correlation Methods*. Halsted Press, Ellis Horwood, Chichester, UK, New York.

Kaufmann, T. & Leonard, E. 1968 Studies of intramembrane transport: A phenomenological approach. *AIChE J.* **14**, 110–117.

Kedem, O. & Katchalsky, A. 1958 Thermodynamic analysis of the permeability of biological membranes to non-electrolytes. *Biochim. Biophys. Acta* **27**, 229–246.

Kedem, O. & Katchalsky, A. 1961 A physical interpretation of the phenomenological coefficients of membrane permeability. *J. Gen. Physiol.* **45**, 143–179.

Kokubo, K. & Sakai, K. 1998 Evaluation of dialysis membranes using a tortuous pore model. *AIChE J.* **44**, 2607–2619.

Koros, W. J., Ma, Y. H. & Shimidzu, T. 1996 Terminology for membranes and membrane processes (IUPAC Recommendations 1996). *J. Membr. Sci.* **120**, 149–159.

Kumins, C. A. & Kwei, T. K. 1968 Free Volume and Other Theories. In: Crank, J. & Park, G. S. (eds) *Diffusion in Polymers*. Academic Press, New York, pp. 107–140.

Lakshminarayanaiah, N. 1969 *Transport Phenomena in Membranes*. Academic Press, New York.

Malone, D. M. & Anderson, J. L. 1978 Hindered diffusion of particles through small pores. *Chem. Eng. Sci.* **33**, 1429–1440.

Marcus, Y. 1985 *Ion Solvation*. John Wiley & Sons, New York.

Meares, P., Thain, J. F. & Dawson, D. G. 1972 Transport across ion-exchange resin membranes: The frictional model of transport. In: Eisenman, G. (ed.) *Membranes: Macroscopic Systems and Models*. Marcel Dekker, New York, pp. 55–124.

Mehdizadeh, H., Dickson, J. M. & Eriksson, P. K. 1989 Temperature effects on the performance of thin-film composite, aromatic polyamide membranes. *Ind. Eng. Chem. Res.* **28**, 814–824.

Mochizuki, S. & Zydney, A. L. 1993 Theoretical analysis of pore size distribution effects on membrane transport. *J. Membr. Sci.* **82**, 211–227.

Nakao, S. 1986 *Membrane Transport Phenomena and Ultrafiltration*. Gulf Publishing Company, Houston, Texas.

Nghiem, L. D., Schafer, A. I. & Elimelech, M. 2004 Removal of the natural hormones by nanofiltration membranes: Measurement, modeling, and mechanisms. *Environ. Sci. Technol.* **38**, 1888–1896.

Schaep, J., Van der Bruggen, B., Uytterhoven, S., Croux, R., Vandecasteele, C., Wilms, D., Van Houtte, E. & Vanlerberghe, F. 1998 Removal of hardness from groundwater by nanofiltration. *Desalination* **119**, 295–302.

Seidel, A., Waypa, J. & Elimelech, M. 2001 Role of charge (Donnan) exclusion in removal of arsenic from water by a negatively charged porous nanofiltration membrane. *Environ. Eng. Sci.* **18**, 105–113.

Sharma, R. R. & Chellam, S. 2005 Temperature effects on morphology of porous thin-film composite nanofiltration membranes. *Environ. Sci. Technol.* **39**, 5022–5030.

Sharma, R. & Chellam, S. 2006 Temperature and concentration effects on electrolyte transport across porous thin film composite nanofiltration membranes: Pore transport mechanisms and energetics of permeation. *J. Colloid Interface Sci.* **298**, 327–340.

Sharma, R. R., Agrawal, R. & Chellam, S. 2003 Temperature effects on sieving characteristics of thin-film composite nanofiltration membranes: Pore size distributions and transport parameters. *J. Membr. Sci.* **223**, 69–87.

Spiegler, K. S. & Kedem, O. 1966 Thermodynamics of hyperfiltration (reverse osmosis): Criteria for efficient membranes. *Desalination* **1**, 311–326.

Szanuawska, D. & Spencer, H. G. 1994 Non-equilibrium thermodynamic analysis of the transport properties of formed-in-place Zr(IV) hydrous oxide-polyacrylate membranes in lactose-water solutions. *Desalination* **95**, 121–137.

Szanuawska, D. & Spencer, H. G. 1997 Non-equilibrium thermodynamics analysis of the transport properties of formed-in-place Zr(IV) hydrous oxide-polyacrylate membranes: III. Ternary lactose-NaCl-water solutions. *Desalination* **113**, 1–6.

Tam, C. M. & Tremblay, A. Y. 1991 Membrane pore characterization: Comparison between single and multicomponent solute probe techniques. *J. Membr. Sci.* **57**, 271–287.

Taniguchi, M. & Kimura, S. 2000 Estimation of transport parameters of RO membranes for seawater desalination. *AIChE J.* **46**, 1967–1973.

Van der Bruggen, B. & Vandecasteele, C. 2002 Modeling of the retention of uncharged molecules with nanofiltration. *Water Res.* **36**, 1360–1368.

Van der Bruggen, B., Schaep, J., Dirk, W. & Vandecasteele, C. 2000 A comparison of models to describe the maximal retention of organic molecules in nanofiltration. *Sep. Sci. Technol.* **35**, 169–182.

Ventresque, C., Turner, G. & Bablon, G. 1997 Nanofiltration: From prototype to full scale. *J. Am. Wat. Wks Assoc.* **89**, 65–76.

Wang, X. -L., Tsuru, T., Togoh, M., Nakao, S.-I. & Kimura, S. 1995a Evaluation of pore structure and electrical properties of nanofiltration membranes. *J. Chem. Eng. Jpn* **28**, 186–192.

Wang, X. -L., Tsuru, T., Nakao, S.-I. & Kimura, S. 1995b Electrolyte transport through nanofiltration membranes by the space-charge model and comparison with Teorell-Meyer-Sievers model. *J. Membr. Sci.* **103**, 117–133.

Washburn, E. W. (ed.) 1929 *International Critical Tables of Numerical Data, Physics, Chemistry and Technology*. McGraw-Hill, New York.

Waypa, J. J., Elimelech, M. & Hering, J. G. 1997 Arsenic removal by RO and NF membranes. *J. Am. Wat. Wks Assoc.* **89**, 102–114.

Wijmans, G. J. & Baker, R. W. 1995 The solution-diffusion model: A review. *J. Membr. Sci.* **107**, 1–21.

Xu, Y. & Lebrun, R. 1999 Investigation of solute separation by charged nanofiltration membrane: Effect of pH, ionic strength and solute type. *J. Membr. Sci.* **158**, 93–104.

Yamauchi, A., Shinozaki, M., Hosoe, L. S. & Miyazaki, M. 1999 Membrane characteristics of composite colloidion membrane I: Water and salt transports across membranes incorporating perfluorobenzoic acid. *J. Membr. Sci.* **163**, 297–305.

Yang, J. -Z. & Liu, J. 1998 Application of Pitzer's electrolyte solution theory to frictional model of charged nanofiltration membrane. *Thermoch. Acta* **308**, 177–182.

First received 15 March 2006; accepted in revised form 20 May 2006